J. Phys. Chem. A **2009,** *113,* 12249–12255

Prediction of Iron-Isotope Fractionation Between Hematite (α-Fe_2O_3) and Ferric and Ferrous Iron in Aqueous Solution from Density Functional Theory

James R. Rustad*,[†] and David A. Dixon[‡]

Department of Geology, University of California, Davis, One Shields Avenue, Davis, California 95616, and Department of Chemistry, University of Alabama, Tuscaloosa, Alabama 35487

Received: July 10, 2009; Revised Manuscript Received: September 16, 2009

Density functional theory electronic structure calculations are used to compute equilibrium constants for iron-isotope exchange among Fe^{2+}(aq), Fe^{3+}(aq), and hematite (α-Fe_2O_3). The hematite is represented in both bulk and surface environments. The iron-isotope fractionation between Fe^{2+}(aq) and Fe^{3+}(aq), determined using a range of exchange-correlation functionals and basis sets, is in good agreement with experimental measurements. The calculated reduced partition function ratio for bulk hematite is very close to previous estimates based on Mössbauer and inelastic nuclear resonance X-ray spectroscopy. However, the calculated fractionation between hematite bulk and the aqueous species Fe^{3+}(aq) and Fe^{2+}(aq) differs from experimental measurements carried out at the aqueous−hematite interface. We find a heavy iron enrichment trend in the order Fe^{2+}(aq) < hematite bulk ≈ hematite surface < Fe^{3+}(aq). In contrast to experimental studies, we find a significant positive fractionation (heavy enrichment) for Fe^{3+}(aq) relative to hematite, regardless of whether the hematite is represented by a bulk or a surface model. Our calculations indicate that it is unlikely that the aqueous interfacial structure of hematite is a simple termination of the bulk structure.

Introduction

At the pH values commonly encountered in low-temperature aqueous systems, Fe^{2+}(aq) coexists with Fe(III) oxide/oxyhydroxide mineral phases at the mineral−water interface. Because of the low solubilities of the ferric oxide phases, Fe^{2+}(aq) is the principal mobile iron species. However, because of the interplay of sorption, hydrolysis, electron transfer, and redissolution, the Fe(II) aqueous−ferric oxide/oxyhydroxide interface is a surprisingly dynamic environment with facile exchange of iron between the mineral and the solution.[1] The rapid shuffling of iron among aqueous species, surface complexes, and oxide phases suggests that equilibrium between the iron isotopes might be readily established in interfacial environments, despite the insolubility of the Fe(III) oxides. The distribution of iron isotopes between aqueous complexes and minerals is an important aid in reconstructing the iron cycle in the early Earth and has important geobiological implications.[2]

Several previous theoretical and experimental studies of iron isotope fractionation are relevant for the Fe^{2+}(aq)−Fe^{3+}(aq)-hematite system.[3−6] In theoretical/empirical studies the equilibrium constant for iron isotope exchange between two iron-bearing hosts, the equilibrium isotope fraction factor (EIFF), is calculated from the ratios of the reduced partition function ratio (RPFR, or, β) for each host. The RPFR for a given host is defined, in the harmonic approximation, as[7]

$$\beta = \prod_i \frac{u_{h_i}}{u_{l_i}} \frac{\exp(-u_{h_i}/2)}{1 - \exp(-u_{h_i})} \frac{1 - \exp(-u_{l_i})}{\exp(-u_{l_i}/2)} \qquad (1)$$

where $u = \hbar c 2\pi\omega/(kT)$, and the $\omega_{(h,l)i}$ are the frequencies of the heavy (h, ^{56}Fe, mass 55.934942) and light (l, ^{54}Fe, mass 53.939615) iron isotopes. These frequencies can be obtained from spectroscopic studies or from electronic structure calculations. The EIFF between species i and j, α_{ij}, is given by β_i/β_j. Theoretical EIFFs estimated in this way are an important complement to direct measurement of isotope distributions using, for example, multicollector inductively coupled plasma mass spectrometry (MC-ICP-MS).[8]

Mössbauer and, more recently, inelastic nuclear resonant X-ray scattering (INRXS) spectroscopic measurements have been used to estimate RPFR values for hematite.[3] Mass spectrometric measurements of the iron-isotope compositions of coexisting Fe^{3+}(aq) and hematite found almost no fractionation between these species.[4] Experimental work on the Fe^{2+}(aq) and Fe^{3+}(aq) system provided measurements of equilibrium fractionation between Fe^{3+}(aq) and Fe^{2+}(aq), giving $\alpha_{aq3aq2} = 1.0030$ at 22 °C.[5] Density functional electronic structure calculations of RFPR values for simple hexaaquo models for Fe^{2+}(aq) and Fe^{3+}(aq) gave α_{aq3aq2} values in good agreement with MC-ICP-MS measurements (~1.00295 at 22 °C).[6] Subsequent density functional theory (DFT) calculations have confirmed these results.[9] However, as previously noted,[6b] the RPFR estimated from DFT calculations, when combined with the Mossbauer/IRNXS estimate[3] of β_{ht} predict Fe^{3+}(aq) to be *enriched* in ^{56}Fe−^{54}Fe relative the hematite by about +1.4 per mil at 98 °C. In contrast, the MC-ICP-MS measurements indicate no fractionation.[4] A potential problem with this analysis is that the computed RPFR values and the RPFR values obtained from Mössbauer/IRNXS spectroscopy may each have a different systematic bias that does not cancel when the EIFF is computed from the RPFR ratios. RPFR values obtained from different techniques, or from calculations using different electronic structure methods, for example, different basis sets and/or DFT potentials, are less likely to be accurate than those calculated from RPFRs obtained from the same technique.

More recent work has focused on more complex systems involving the fractionation of iron isotopes between Fe^{2+}(aq)

---

* To whom correspondence should be addressed. E-mail: jrrustad@ucdavis.edu.

[†] University of California.

[‡] University of Alabama.

10.1021/jp9065373 CCC: $40.75

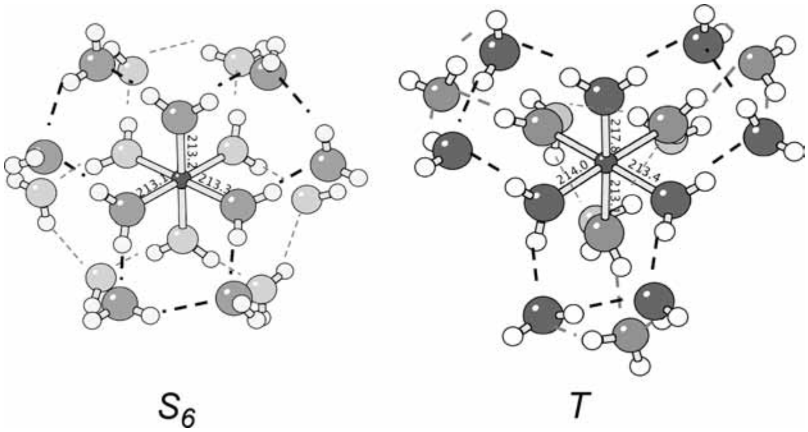

Figure 1. Structural models of $Fe(H_2O)_{18}{}^{n+}$ for $n = 2$ and 3 used to represent the Fe^{2+}(aq) and Fe^{3+}(aq) species. Small dark atoms, Fe; small light atoms, H; large atoms, O. Hydrogen bonds between water molecules are given by dashed lines. Bond lengths for Fe^{2+}(aq) are given in picometers to give a sense of the differences in Fe−O bond distortion. S_6 and T are actual symmetries for the Fe^{3+}(aq) complexes, but only approximate for the Fe^{2+}(aq) complexes run in C_1 point group symmetry.

and α-Fe_2O_3 in the presence of iron-reducing bacteria.[10] These studies focused on the isotopic fractionation between the Fe^{2+}(aq) produced by biogenic iron reduction and the hematite on which the bacteria were grown. The measured $^{56}Fe-^{54}Fe$ fractionation between hematite and biogenic Fe^{2+}(aq) was essentially identical to the measured value[5] of $\alpha_{\text{aq3-aq2}}$, consistent with experiments in ref 4, indicating nearly zero fractionation between Fe^{3+}(aq) and hematite.

Following previous DFT investigations of the Fe^{2+}(aq)−Fe^{3+}(aq) system,[6,9] we use electronic structure calculations at the same DFT level in terms of the basis set and exchange-correlation functional to predict RPFRs for Fe^{2+}(aq), Fe^{3+}(aq), bulk hematite, and two models of the hematite (012) surface. With these calculations, it is possible to estimate both $\alpha_{\text{ht-aq2}}$ and $\alpha_{\text{aq3-ht}}$ using reduced partition function ratios obtained from the same theoretical method. By allowing for cancellation of possible systematic errors, this approach should provide a more reliable estimate than using the ratios of RPFR values obtained spectroscopically for hematite and theoretically for $Fe^{2+/3+}$(aq), or using the ratios of RPFR values obtained using different theoretical methods.

Methods

Model Systems. Two structural models, shown in Figure 1, are used to represent the aqueous complexes Fe^{2+}(aq) and Fe^{3+}(aq). Both models include the hexaaquo complex plus 12 waters representing the second solvation shell ($Fe(H_2O)_{18}{}^{3+}$ and $Fe(H_2O)_{18}{}^{2+}$); thus each of the protons on the inner shell water molecules is hydrogen-bonded to a second shell water molecule. This type of model has been shown to give reliable results for the prediction of the equilibrium between $UO_2{}^{2+}(H_2O)_5$ and $UO_2{}^{2+}(H_2O)_4$ in aqueous solution, for example.[11] For Fe^{3+}(aq), these structures have S_6 and T point group symmetry. For Fe^{2+}(aq) the symmetry is only approximate as the optimized structure has C_1 symmetry and the Fe−O bond lengths distort from the ideal symmetry group, especially for the T conformer (see Figure 1).

An embedded cluster model is used to represent the crystallographic environments of iron atoms in bulk hematite and at the hematite surface. There are important advantages for the embedded cluster approach for this problem. First, one can use standard all-electron quantum chemistry techniques, avoiding the construction and testing of a pseudopotential for iron. Second, one can readily employ hybrid functionals, with some component of exact exchange, in the DFT calculations. In contrast, computing exact exchange contributions in a plane wave basis is computationally expensive. Among other features, exact exchange can be important for obtaining reasonable band gaps in solids.[12] Obvious disadvantages of the cluster approach are the neglect of (1) the phonon contributions to the fractionation and (2) the role of the Madelung contribution to the potential energy surface of the vibrating atom undergoing isotope exchange. Through proper construction of neutral clusters, the latter effect can be minimized. The phonon contributions do not appear to be large in systems where comparisons can be made between the embedded cluster calculations and fully periodic calculations.[13]

The embedded cluster approach uses a "free" core optimized in a rigid shell of oxygen atoms fixed in their measured lattice positions. The vibrational frequencies of the free core within the rigid shell are used to compute the RPFR in the harmonic approximation using eq 1. Following our previous studies of EIFFs in solids using cluster models,[13] the connection between the rigid oxygen shell and the outside cluster is represented by "quasi-atoms" placed along each "clipped" Fe−O bond with a core charge equal to the Pauling bond valence (charge divided by coordination number) contributed by the clipped Fe atom (always $+^3/_6 = {}^1/_2$ in the case of the cluster representing bulk hematite). Our approach, which, by construction, always produces a neutral cluster, is similar in spirit to the method used by Evjen to compute lattice energies of crystals.[14] The "free" core of the cluster representing the bulk (Figure 2a) consists of a central Fe_2O_3 "molecule", with six additional oxygen atoms completing the octahedral coordination shell of the two iron atoms. All iron atoms attached to these nine oxygen atoms, beyond those in the central Fe_2O_3 unit, are included in the core cluster. There are thus a total of 20 iron atoms in the electronic structure calculations, and the high spin electronic state was chosen with 100 unpaired electrons from 20 high spin Fe^{3+} with 5 unpaired electrons in each of the 5 3d orbitals. All oxygen atoms bound to the 18 iron atoms outside the central Fe_2O_3 molecule, that is, those oxygen atoms completing the octahedral coordination polyhedra of the iron atoms, but not among the 9 core oxygen atoms, are fixed in their lattice positions[15] (51 noncore oxygen atoms total) and terminated on the outside by the Pauling bond strength-conserving quasi-atoms (120 total) as described above.

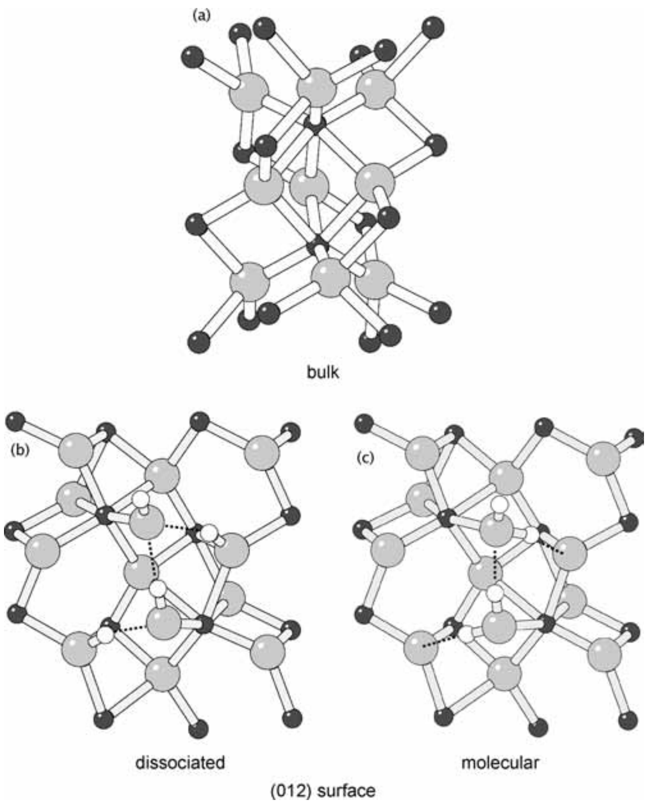

Figure 2. Core component of model cluster used to represent bulk hematite (a), and the hematite (012) surface (b, dissociated; c, molecular) in the electronic structure calculations. Small dark atoms, Fe; small light atoms, H; large atoms, O. Oxygen atoms in the embedding region are not shown, but complete the coordination shells of the iron atoms that lack six coordinating oxygen atoms in the figure.

The (012) surface of hematite has been well studied experimentally under high vacuum conditions[16] and in solution.[17] The cores of the surface structural models, based on a stoichiometric termination of the bulk hematite structure, are shown in Figure 2b,c. Both consist of the two unique iron octahedra in the surface unit cell of hematite using the vacuum termination obtained from experiment,[16] all of the iron atoms bound to the oxygen atoms comprising the two octahedra, and two adjacent triply bridging oxygen atoms, making a total of 16 iron atoms, 13 oxygen atoms, and 4 hydrogen atoms in the core. Again, the oxygen atoms bound to the second-shell iron atoms, but not already included in the set of core oxygen atoms, are fixed in their ideal (bulk) lattice positions (a total of 32 noncore oxygen atoms) and terminated with Pauling bond strength-conserving quasi-atoms as described above (74 total quasi-atoms). Each of the 16 iron atoms was constrained in the high-spin state, with a total number of 80 unpaired electrons. The two surface conformers were obtained in a search procedure starting from 32 different structures, including completely undissociated, half-dissociated, and fully dissociated water configurations, scanning over OH groups in all different possible orientations defined by the Fe−O bonds that were broken when the surface was cleaved.

In the lowest-energy conformer (Figure 2b), the sorbed water molecules are fully dissociated into singly coordinated OH^- ions in the central part of the core. The H^+ ions given up by the sorbed waters are bonded to the triply coordinated lattice oxygen atoms. We also consider a conformer with adsorbed waters intact in the molecular state. The conformer in Figure 2c was the lowest-energy conformer with molecularly absorbed water. Energetically, this conformer is 2.5 (PBE/DZP), 4.5 (BLYP/DZP), and 5 (B3LYP/DZP) kcal/mol above the fully dissociated conformer in Figure 2b. Actual hematite surfaces with one monolayer of sorbed water are about 75% dissociated as determined by temperature-programmed desorption experiments and the observed extent of mixing of oxygen isotopes between the surface and a monolayer of sorbed water.[16] The Cartesian coordinates of all atoms and terminating quasi-atoms for the clusters illustrated in Figure 2a,b are given in the Supporting Information.

Electronic Structure Calculations. The structures were optimized using the PQS quantum chemistry package[18] and vibrational frequencies were obtained from the Hessian matrix calculated analytically on the fully optimized structure. Integral thresholds and optimization tolerances were increased an order of magnitude beyond default values, and an extra fine grid was used for numerical integration of the DFT exchange-correlation functional. The tighter convergence criteria typically make a (nonsystematic) difference of 0.1−0.2 per mil in the calculated RPFR. For the hematite structures, a partial Hessian was extracted by removing the rows and columns corresponding to the fixed oxygen atoms in the embedding region. The partial Hessian was diagonalized using the Jacobi method. Doing this last step “by hand” (outside the PQS code), is necessary to avoid projecting out the rotational and translational modes, which is done automatically in many electronic structure codes. These modes, of course, are not present at zero frequency in the embedded cluster used to model the solid state and should not be projected out.

For the aqueous systems, the following basis sets were used: DZP (polarized double ζ), 6-31G* on O and H, *m*6-31G* Fe;[19] ADZP (diffuse function + polarized double ζ), 6-31+G* on O and H, *m*6-31G* on Fe; and ATZP (diffuse function + polarized triple ζ), 6-311++G** on O and H, the Wachters basis set on Fe.[20] The calculations were done with several commonly used exchange-correlation functionals: the hybrid functionals including some component of Hartree−Fock exchange, B3LYP[21] and B97−1;[22] the GGA functionals BLYP[23] and BPW91,[23a,24] and the “second-generation” GGA functionals PBE,[25] OLYP,[26,23b] and HCTH-407.[27] For the hematite bulk and hematite surface calculations, the 3-21G basis set was used for the embedding region, including hydrogen basis functions on the 0.5*e* quasi-atoms for the bulk cluster and 0.513513513*e* for the surface cluster (the charge necessary to obtain a neutral cluster). The core region of the embedded cluster is treated using the DZP basis set described above. The bulk and surface calculations (1554 and 1476 uncontracted Gaussian basis functions at the DZP level, respectively) are much larger than the $Fe(OH_2)_{18}$ aqueous ions, (378 contracted gaussians at the DZP level). Thus the bulk and surface clusters were run only with the DZP basis set with the B3LYP, PBE, and BLYP functionals.

The reduced partition function ratios were calculated using the unscaled frequencies. An important reason for scaling frequencies is to make the calculated harmonic frequencies agree better with the measured anharmonic frequencies. Since the harmonic approximation is used to evaluate the reduced partition function ratio, it is more consistent to use unscaled calculated frequencies in these calculations.[6] The Redlich−Teller sum,[28] $\ln \Pi_i(\omega_{li}/\omega_{hi})$, for the embedded cluster was within 1 part in 10^8 of $^3/_2 \ln(55.934942/53.939615)$, as it should be for a system with neither translational nor rotational kinetic energy.

Results

The results of the calculations on each of the two conformers for both $Fe^{2+}(aq)$ and $Fe^{3+}(aq)$ are given in Table 1 for the three

TABLE 1: Reduced Partition Function Ratios and Equilibrium Constants for $^{56}Fe^{3+}(aq) + {}^{54}Fe^{2+}(aq) \rightleftharpoons {}^{54}Fe^{3+}(aq) + {}^{56}Fe^{2+}(aq)$ at 25 °C

	DZP			ADZP			ATZP		
DFT/V_{XC}	β(Fe(III))	β(Fe(II))	α_{aq3aq2}	βFe((III))	βFe((II))	α_{aq3aq2}	βFe((III))	βFe((II))	α_{aq3aq2}
				S_6 Model for $Fe(H_2O)_{18}{}^{n+}$					
B3LYP	1.0092	1.0059	1.0033	1.0088	1.0054	1.0034	1.0085	1.0051	1.0034
B971	1.0093	1.0056	1.0037	1.0088	1.0053	1.0033	1.0086	1.0051	1.0035
BLYP	1.0080	1.0054	1.0026	1.0075	1.0050	1.0025	1.0072	1.0046	1.0026
BPW91	1.0085	1.0055	1.0030	1.0078	1.0051	1.0027	1.0076	1.0047	1.0029
HCTH	1.0077	1.0048	1.0029	1.0071	1.0044	1.0027	1.0070	1.0040	1.0030
OLYP	1.0076	1.0048	1.0028	1.0070	1.0044	1.0026	1.0068	1.0038	1.0030
PBE	1.0086	1.0056	1.0030	1.0079	1.0052	1.0027	1.0076	1.0048	1.0028
				T Model for $Fe(H_2O)_{18}{}^{n+}$					
B3LYP	1.0090	1.0054	1.0036	1.0085	1.0046	1.0038	1.0082	1.0044	1.0038
B971	1.0093	1.0055	1.0038	1.0086	1.0048	1.0038	1.0083	1.0046	1.0037
BLYP	1.0078	1.0050	1.0028	1.0072	1.0041	1.0031	1.0069	1.0038	1.0031
BPW91	1.0080	1.0051	1.0029	1.0076	1.0042	1.0034	1.0073	1.0044	1.0029
HCTH	1.0074	1.0044	1.0030	1.0069	1.0038	1.0031	1.0069	1.0036	1.0033
OLYP	1.0073	1.0043	1.0030	1.0071	1.0036	1.0035	1.0067	1.0037	1.0030
PBE	1.0083	1.0053	1.0030	1.0078	1.0044	1.0033	1.0075	1.0041	1.0034

TABLE 2: Reduced Partition Function Ratios ($^{56}Fe-{}^{54}Fe$) for Hematite Bulk and Surface Iron Atoms Calculated Using B3LYP, PBE, and BLYP Exchange-Correlation Potentials at 25 and 100 °C

system	T (°C)	β (B3LYP)	β (PBE)	β (BLYP)	ref 3b	ref 33[b]
hematite bulk	25	1.0079	1.0069	1.0070	1.0078	1.0071
hematite (012) dissociated	25	1.0080	1.0069	1.0068		
		1.0080	1.0069	1.0068		
hematite (012) molecular	25	1.0078[a]	1.0067	1.0066		
		1.0076	1.0066	1.0064		
hematite bulk	100	1.0052	1.0045	1.0046	1.0044	1.0041
hematite (012) dissociated	100	1.0052	1.0045	1.0044		
		1.0052	1.0045	1.0044		
hematite (012) molecular	100	1.0051[a]	1.0044	1.0043		
		1.0049	1.0043	1.0041		
$Fe^{3+}(aq)$ S_6	100	1.0060	1.0056	1.0053		
$Fe^{2+}(aq)$ S_6	100	1.0039	1.0037	1.0035		
$Fe^{3+}(aq)$ T	100	1.0059	1.0054	1.0051		
$Fe^{2+}(aq)$ T	100	1.0035	1.0035	1.0032		

[a] The iron atom attached to the hydrogen-bond accepting water (top, Figure 2c) is slightly heavier than hydrogen bond-donating water (bottom, Figure 2c). [b] Periodic density functional calculations using the PBE exchange-correlation functional.

basis sets and the seven exchange-correlation functionals. Table 1 gives RPFRs both for $Fe^{2+}(aq)$ and $Fe^{3+}(aq)$ as well as the predicted equilibrium constant $\alpha_{aq3\text{-}aq2}$ for the reaction

$$^{56}Fe^{3+}(aq) + {}^{54}Fe^{2+}(aq) \rightleftharpoons {}^{54}Fe^{3+}(aq) + {}^{56}Fe^{2+}(aq) \quad (2)$$

The RPFRs themselves are sensitive to both the basis set and the solvent representation. In particular, the OLYP and HCTH/407 functionals give low RPFR values. However, there is a significant cancellation of errors, and the predicted $\alpha_{aq3\text{-}aq2}$ are less dependent on the particular exchange-correlation functional used in the DFT calculations. The variation in $\alpha_{aq3\text{-}aq2}$ with respect to the choice of exchange-correlation functional is still significant, however, with the hybrid functionals predicting $\alpha_{aq3\text{-}aq2}$ up to 1 per mil higher than the pure GGA functionals. The BLYP functional consistently gives the lowest $\alpha_{aq3\text{-}aq2}$ values. Predicted fractionations for the T conformer are up to 0−0.5 per mil higher than the S_6 conformer, depending on the functional used. The predicted EIFF has only a small dependence on the basis set for a given functional.

The value for $\alpha_{aq3\text{-}aq2}$ calculated using the B3LYP functional and the 6-31G* basis set is nearly 1 per mil higher than previous studies.[6] This difference is primarily due to the RPFR for $Fe^{2+}(aq)$ being ∼1 per mil lower than in the previous work. The main differences between the calculations presented here and those in ref 6 are that the previous work used the Ahlrichs triple-ζ basis set for Fe[29] and used a continuum solvent representation instead of an explicit second shell. The difference in the calculated values of $\alpha_{aq3\text{-}aq2}$ is most likely due to the basis set used in the previous work, as the difference persists if the COSMO continuum solvation model is used,[30] and also if only the gas-phase $Fe(H_2O)_6{}^{2+}$ complex (without the explicit second shell waters) is treated.

Although the best agreement with the measured $\alpha_{aq3\text{-}aq2}$ is given by the GGA functionals, it would be premature to conclude that these are necessarily better for this system until a more thorough analysis of the vibrational spectrum has been carried out, preferably in the alum[31] and Tutton[32] salt crystal environments for which the experimental data are clearer than in solution, and until there is a better understanding of the magnitude of anharmonic contributions.

RPFR values at 25 °C for the iron atoms in the core of the bulk hematite cluster are given in Table 2 for the B3LYP, PBE, and BLYP functionals. Although the two core iron atoms in the model for the surface are not symmetrically equivalent, they differ in RFPR by less than 0.00001 for a given functional, so separate RFPRs are not reported. As shown in Table 2, at 25 °C, the Mössbauer/IRNXS-derived RPFR[3b] is in good agreement

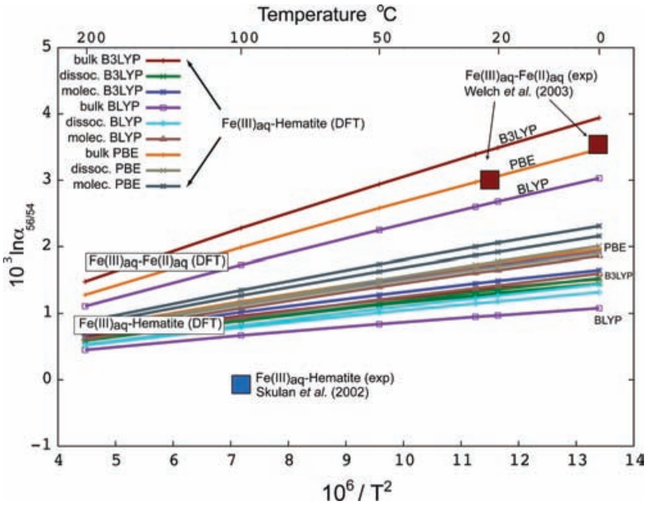

Figure 3. Summary of density functional calculations performed in this study versus experimental measurements for ^{56}Fe−^{54}Fe fractionation between Fe^{3+}(aq)−Fe^{2+}(aq) (above) and Fe^{3+}(aq)−hematite bulk and surface environments (below). Results are shown only for the S_6 aqueous conformer. Two lines are given for molecular and dissociated surface structures because the iron atoms in the clusters are not equivalent. For the bulk cluster, the differences between the iron atoms are too small to be apparent on the figure.

with our calculated values, with the best agreement resulting for the B3LYP functional. The temperature dependence may be slightly underestimated by the DFT calculations. The GGA calculations are in good agreement with fully periodic GGA calculations.[33] As is the case for the carbonate[13a] and ferropericlase/ferroperovskite systems,[13b] the cluster approximation gives reasonable accuracy for computing RPFRs.

Calculations on the model systems representing the hematite (012) surface are also given in Table 2. Again, the two core iron atoms are not symmetrically equivalent, but have small differences in their RFPR. Even for the conformer with molecularly absorbed water molecules where one of the molecules is a hydrogen-bond acceptor and one is a donor, the difference in the RFPR values of the two core iron atoms is small (0.2 per mil). The differences the RPFR between the dissociated and molecular conformers is also small, with the molecular conformer about 0.2−0.4 per mil lighter than the dissociated conformer. For the purposes of this analysis, there is essentially no difference between the DFT-calculated hematite surface and bulk RPFRs; both hematite bulk and surface environments (as modeled here) can, for all practical purposes, be considered as hematite.

Comparing the RPFRs between the aqueous species and solid-state and surface environments, we find that Fe^{3+}(aq) is isotopically heaviest, followed by hematite, with (as expected) Fe^{2+}(aq) being isotopically lightest. The predicted fractionations of Fe^{3+}(aq) (S_6 conformer) with respect to hematite are illustrated graphically in Figure 3. Numerical values for the fractionation of bulk hematite against Fe^{2+}(aq) and Fe^{3+}(aq) are given in Table 3 using the RPFR values of the aqueous species taken from Table 1. Note that in Table 3, all α values are positive, being given as $\alpha_{\text{aq3-ht}}$ and $\alpha_{\text{ht-aq2}}$. Fe^{3+}(aq) is isotopically heavier than hematite by 0.7−1.7 per mil at 25 °C (with the PBE functional predicting a greater extent of fractionation). At 100 °C, this is lowered slightly to 0.5−1.1 per mil. These ranges expand only slightly if surface species are considered (see Figure 3). Because the hematite surface is approximately 75% dissociated, the signature of the dissociated surface, which is somewhat closer to the bulk than the surface with molecularly absorbed waters, may be more relevant.

In comparing the results across different functionals, it is notable that the PBE functional predicts hematite RPFR values that are very similar to BLYP, whereas, for the aqueous species, the RPFR values are intermediate between B3LYP and BLYP. Thus, in an overall sense, the PBE functional tends to predict $\alpha_{\text{aq3-ht}}$ values that are higher than the other two functionals. As shown in Figure 3, all DFT predictions, however, are well above the measured value, regardless of the exchange-correlation functional used.

Discussion

The predicted ^{56}Fe−^{54}Fe enrichment in Fe^{3+}(aq) relative to hematite is surprising because the bonding environment would be expected, roughly speaking, to be stiffer in the crystal than in aqueous solution. Some insight into this issue is shown in Figure 4, in which the cumulative contributions to the RPFR are plotted as a function of frequency for both S_6 and T conformers of Fe^{3+}(aq) and hematite surface (dissociated conformer) and bulk clusters. Although the contributions are more spread-out for the solid species, being less localized in the stretching and bending regions, the aqueous and solid-state values are close to one another at ∼800 cm^{-1}. The RPFR values for the hematite species show little increase after 700 cm^{-1}. In contrast, there are significant contributions made by the water wagging motions near 1030 cm^{-1} in the S_6 aqueous cluster. For the T cluster, these contributions occur at lower frequencies and are not as well resolved into particular vibrational modes, but give a similar overall contribution to the RPFR. Thus, when evaluating the possible crystallographic environmental influences governing the fractionation, it is important to consider the contributions of higher frequency vibrational modes that are still low enough to couple to some extent with the main fractionating vibrational modes (in this case, the octahedral O−Fe−O bend and Fe−O stretching vibrations between 450−500 cm^{-1}). Because the highest frequency in the hematite bulk cluster is less than 700 cm^{-1}, there is no possibility of coupling with higher frequency modes to raise the RPFR. Similar behavior was noted in the minerals ferropericlase ($Fe_xMg_{(1-x)}O$) and ferroperovskite ($Fe_xMg_{(1-x)}SiO_3$) systems,[13b] where the Si−O stretching frequencies couple with the Fe−O stretching frequencies in ferroperovskite to raise the RPFR above that for ferropericlase, even though the Fe−O bonds are shorter for ferropericlase than for ferroperovskite. One might then expect the hematite surface to be enriched in heavy iron relative to the bulk; however, the restricted motions of the hydroxide ions do not couple strongly to the iron vibrations at the surface for either the dissociative or molecular conformers and thus do not contribute to the RFPRs.

The DFT calculations presented here indicate that even when all RPFR values are derived from a common type of electronic structure calculation, Fe^{3+}(aq) is enriched in ^{56}Fe−^{54}Fe relative to hematite by 0.7−1.7 per mil at 25 °C and by 0.5−1.1 per mil at 100 °C, regardless of whether the surface or bulk structure is considered as the model the hematite crystallographic environment. The ^{56}Fe−^{54}Fe enrichment of hematite relative to Fe^{2+} is calculated to be 1.3−2.6 per mil at 25 °C, which is 1−2 per mil below the measured values.[10] Because the Fe^{2+}(aq)/Fe^{3+}(aq) fractionation is well described by a variety of DFT functionals and basis sets, and we have chosen the DFT functionals showing the greatest range in the predicted $\alpha_{\text{aq3-aq2}}$, it seems unlikely that the discrepancy with the measured fractionations arises because of the choice of the exchange-

TABLE 3: Isotope Fractionation Factors (^{56}Fe−^{54}Fe) Calculated for Hematite Bulk Relative to Fe^{2+}(aq) and Fe^{3+}(aq) at 25 °C

		B3LYP		PBE		BLYP	
	T (°C)	*T*	S_6	*T*	S_6	*T*	S_6
$\alpha_{\text{ht-aq2}}$	25	1.0026	1.0020	1.0016	1.0013	1.0021	1.0017
$\alpha_{\text{aq3-ht}}$	25	1.0010	1.0012	1.0014	1.0017	1.0007	1.0010
$\alpha_{\text{aq3-ht}}$	100	1.0007	1.0009	1.0010	1.0011	1.0005	1.0007

correlation functional in the DFT calculations. It is also unlikely to result from basis set incompleteness, as we have shown that the basis set makes only a small difference for the aqueous complexes of these cationic species.

Because our calculated 25 °C RPFR values for hematite are close to the empirically estimated values[3] as well as those obtained from fully periodic DFT calculations,[33] it is unlikely that the discrepancy between the measured and calculated Fe^{3+}(aq)-hematite fractionation is an artifact of the embedded cluster model, nor conversely from an unrecognized systematic error in the Mössbauer-derived RPFR. In fact, our computed $\alpha_{\text{aq3-ht}}$ at 100 °C (1.0005−1.0011), depending on the solvent conformation and the exchange-correlation functional (see Table 3 and Figure 3), is not much different from the estimate of 1.0014 given previously[6b] using a DFT-calculated value for the RPFR of Fe^{3+}(aq) together with the Mössbauer-derived RPFR. The near equality of the calculated surface and bulk values for hematite also argues against the observed fractionations being strongly dependent on the choice of a structural model for hematite. Furthermore, the calculations show that there are good physical reasons to expect the RPFR value for Fe^{3+}(aq) to be higher than that of hematite because of the coupling with higher frequency motions that are absent in the solid, at least in the bulk hematite cluster.

On the other hand, given the consistency between the measured values for $\alpha_{\text{aq3-ht}}$,[4] $\alpha_{\text{ht-aq2}}$,[10] and $\alpha_{\text{aq3-aq2}}$,[5] it is not easy to argue for misinterpretation of the experimental studies, despite the significant technical challenges involved in the extraction of distinct isotopic pools in the interfacial environment. One possibility is that the experimental studies are recording a nonequilibrium component in the observed fractionation. However, the experimental studies have made impressive efforts to eliminate time-dependence from their measurements, so this seems unlikely. Another possibility is that the iron environment at the hematite surface is different from either the bulk or the vacuum termination used to construct the model for the surface. For example, the reaction of water with hematite could, over time, produce a passivating hydration layer on hematite, possibly inducing iron vacancies according to the "hydrohematite" substitution[34] ($3H^+$ exchanged for Fe^{3+}), possibly resulting in a structure more similar to Fe^{3+}(aq) (i.e., more than a single bound OH^- or H_2O per iron atom), giving hematite an isotopic signature closer to Fe^{3+}(aq).

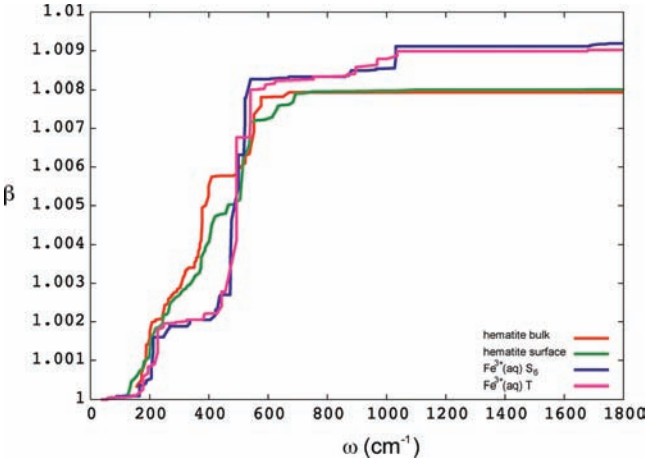

Figure 4. Cumulative contributions to the reduced partition function ratio β (eq 1) as calculated with the B3LYP exchange-correlation functional. Results are given as a function of frequency for Fe^{3+}(aq) S_6 (blue); Fe^{3+}(aq) *T* (magenta); hematite bulk (red); hematite (012) surface, dissociated conformation (green).

It is important to stress that in the cases where the chemical species involved in the fractionation are known most precisely, namely, the Fe^{3+}(aq) and Fe^{2+}(aq) systems and the hematite bulk environment, the agreement between the measured (aqueous EIFF) and empirical/experimental (hematite RPFR) fractionations and the DFT calculations is good. The most direct way to resolve the discrepancies highlighted here would be to perform mass-spectrometric measurements of iron isotope distributions on systems of known structure, perhaps analogous to the polyoxocation materials which have properties intermediate between aqueous complexes and surfaces.[35] It is in these systems, where structures are characterized most completely, that comparisons between theory and experiment would be the most revealing.[36] Establishing a predictive relationship between structure and isotopic composition, along the lines of the hematite-Fe^{3+}(aq) system explored here, could be used to invert the problem, allowing isotopic signatures to serve as an indicator of surface structure in complex interfaces, especially where structural characterization is difficult.[37] To some extent, this concept can be applied to the current study, in the sense that the calculations presented here effectively rule out the possibility that the measured interfacial isotope distributions reflect equilibrium fractionation between solution and bulk hematite, or between solution and a hematite surface resembling a stoichiometric termination of the bulk structure. It would be interesting to carry out DFT calculations on the nonstoichiometric termination[17] to see if this surface would carry a heavier iron isotope signature; however, given the similarity between the predicted fractionations in the bulk and the stoichiometric (012) termination, and the insensitivity to the extent of water dissociation on the surface, this seems unlikely. In other words, qualitatively speaking, the structural differences between the nonstoichiometric surface and the stoichiometric surface do not appear to be larger than those between the stoichiometric surface and the bulk. The large difference between the predicted and measured fractionations probably indicates a strong structural difference in the interfacial environment.

Conclusions

Density functional theory calculations of the reduced partition function ratios for ^{56}Fe−^{54}Fe exchange on bulk hematite and for the (012) hematite surface, in conjunction with those calculated for Fe^{2+}(aq) and Fe^{3+}(aq), with a range of exchange-correlation functionals, indicate that hematite should lie between Fe^{3+}(aq) (heaviest) and Fe^{2+}(aq) (lightest) in terms of heavy isotope enrichment. The predicted fractionation between aqueous species Fe^{2+}(aq) and Fe^{3+}(aq) is in good agreement with mass-spectrometric measurements.[5] The calculated reduced partition function ratio of hematite is in good agreement with estimates based on Mössbauer and inelastic nuclear resonant X-ray spectroscopy.[3] We find nearly identical reduced partition function ratios for iron residing in bulk hematite and at the (012) hematite surface, indicating that surface-induced fractionation effects are small. We also find that surface conformers having molecularly and dissociatively adsorbed water molecules have similar reduced partition function ratios. Plots of the cumulative reduced partition function ratio as a function of frequency show that the heavy isotope enrichment for Fe^{3+}(aq) is primarily due to coupling of the octahedral Fe−O stretching and O−Fe−O bending motions between 450 and 500 cm^{-1} with the wagging vibrations of bound water molecules at frequencies between 800 and 1100 cm^{-1}. The discrepancy between the calculated and measured interfacial iron isotope fractionation should encourage detailed structural investigations of the hematite surfaces on which isotope fractionation measurements have been carried out. Given the accuracy demonstrated for the calculations, it is unlikely that the hematite structure at the hematite−water interface resembles a simple termination of the bulk structure. Coupled with theoretical calculations, experimental measurements of isotopic composition of iron oxide surfaces provide more valuable information concerning their surface structures than previously thought.

Acknowledgment. The National Science Foundation Grant EAR0814242 (J.R.R.) and the Chemistry and Geosciences Division, Office of Basic Energy Sciences, United States Department of Energy (DAD) supported this work. The authors are grateful to Prof. Clark M. Johnson for valuable comments on the manuscript.

Supporting Information Available: Optimized geometries and total energies using B3LYP/ATZP are given for aqueous complexes and B3LYP/DZP for hematite surface with dissociatively adsorbed water molecules and bulk. Calculated vibrational frequencies are give for all functionals with ATZP basis for aqueous complexes; B3LYP and BLYP functionals with DZP basis set for hematite surface and bulk. This material is available free of charge via the Internet at http://pubs.acs.org.

References and Notes

(1) (a) Williams, A. G. B.; Scherer, M. M. *Environ. Sci. Technol.* **2004**, *38*, 4782. (b) Pedersen, H. D.; Postma, D.; Jakobsen, R.; Larsen, O. *Geochim. Cosmochim. Acta* **2005**, *69*, 3967. (c) Yanina, S. V.; Rosso, K. M. *Science* **2008**, *320*, 218. (d) Handler, R. M.; Beard, B. L.; Johnson, C. M.; Scherer, M. M. *Environ. Sci. Technol.* **2009**, *43*, 1102.

(2) (a) Anbar, A. D. *Earth Planet. Sci. Lett.* **2004**, *217*, 223. (b) Anbar, A. D.; Rouxel, O. *Ann. Rev. Earth Planet. Sci.* **2007**, *35*, 717. (c) Johnson, C. M.; Beard, B. L.; Roden, E. E. *Ann. Rev. Earth Planet. Sci.* **2008**, *26*, 457.

(3) (a) Polyakov, V. B.; Mineev, S. D. *Geochim. Cosmochim. Acta* **2000**, *64*, 849. (b) Polyakov, V. B.; Clayton, R. N.; Horita, J.; Mineev, S. D. *Geochim. Cosmochim. Acta* **2007**, *71*, 3833.

(4) Skulan, J. L.; Beard, B. L.; Johnson, C. M. *Geochim. Cosmochim. Acta* **2002**, *66*, 2995.

(5) (a) Johnson, C. M.; Skulan, J. L.; Beard, B. L.; Sun, H.; Nealson, K. H.; Braterman, P. S. *Earth Planet. Sci. Lett.* **2002**, *195*, 141. (b) Welch, S. A.; Beard, B. L.; Johnson, C. M.; Braterman, P. S. *Geochim. Cosmochim. Acta* **2003**, *67*, 4231.

(6) (a) Jarzecki, A. A.; Anbar, A. D.; Spiro, T. G. *J. Phys. Chem. A* **2004**, *108*, 2726. (b) Anbar, A. D.; Jarzecki, A. A.; Spiro, T. G. *Geochim. Cosmochim. Acta* **2005**, *69*, 825.

(7) (a) Urey, H. C. *J. Chem. Soc.* **1947**, 562. (b) Bigeleisen, J.; Mayer, M. G. *J. Chem. Phys.* **1947**, *15*, 261.

(8) Schauble, E. A. *MSA Rev. Miner. Geochem.* **2004**, *55*, 65.

(9) (a) Hill, P. S.; Schauble, E. A. *Geochim. Cosmochim. Acta* **2008**, *72*, 1939. (b) Domagal-Goldman, S. D.; Kubicki, J. D. *Geochim. Cosmochim. Acta* **2008**, *72*, 5201. (c) Domagal-Goldman, S. D.; Paul, K. W.; Sparks, D. L.; Kubicki, J. D. *Geochim. Cosmochim. Acta* **2009**, *73*, 1.

(10) (a) Crosby, H. A.; Johnson, C. M.; Roden, E. E.; Beard, B. L. *Environ. Sci. Technol.* **2005**, *39*, 6698. (b) Crosby, H. A.; Roden, E. E.; Johnson, C. M.; Beard, B. L. *Geobiology* **2007**, *5*, 169.

(11) Gutowski, K. E.; Dixon, D. A. *J. Phys. Chem. A* **2006**, *110*, 8840.

(12) Martin, R. L.; Illas, F. *Phys. Rev. Lett.* **1997**, *79*, 1539.

(13) (a) Rustad, J. R.; Nelmes, S. L.; Jackson, V. E.; Dixon, D. A. *J. Phys. Chem. A* **2008**, *112*, 542. (b) Rustad, J. R.; Yin, Q.-z. *Nat. Geoscie.* **2009**, *2*, 514.

(14) Evjen, H. M. *Phys. Rev.* **1932**, *39*, 675.

(15) Gaultieri, A.; Venturelli, P. *Am. Mineral.* **1999**, *84*, 295.

(16) Henderson, M. A.; Joyce, S. A.; Rustad, J. R. *Surf. Sci.* **1998**, *417*, 66.

(17) Tanwar, K. S.; Catalano, J. G.; Petitto, S. C.; Ghose, S. K.; Eng, P. J.; Trainor, T. P. *Surf. Sci.* **2007**, *601*, L59.

(18) http://www.pqschem.com (version 3.3, June, 2008).

(19) Mitin, A. V.; Baker, J.; Pulay, P. *J. Chem. Phys.* **2003**, *118*, 7775.

(20) Wachters, A. J. H. *J. Chem. Phys.* **1970**, *52*, 1033.

(21) Becke, A. D. *J. Chem. Phys.* **1993**, *98*, 5648.

(22) Becke, A. D. *J. Chem. Phys.* **1997**, *107*, 8554.

(23) (a) Becke, A. D. *Phys. Rev. A* **1988**, *38*, 3098. (b) Lee, C.; Yang, W.; Parr, R. G. *Phys. Rev. B* **1988**, *37*, 785.

(24) Perdew, J. P.; Wang, Y. *Phys. Rev. B* **1991**, *45*, 13244.

(25) Perdew, J. P.; Burke, K.; Ernzerhof, M. *Phys. Rev. Lett.* **1996**, *77*, 3865.

(26) Handy, N. C.; Cohen, A. *J. Mol. Phys.* **2001**, *99*, 403.

(27) Boese, A. D.; Handy, N. C. *J. Chem. Phys.* **2001**, *114*, 5497.

(28) Herzberg, G. *Molecular Spectra and Molecular Structure: Infrared and Raman Spectra of Polyatomic Molecules*; van Nostrand Reinhold: New York, 1945; pp 231−238. (b) Teller, E.; Angus, W. R.; Bailey, C. R.; Hale, J. B.; Ingold, C. K.; Leckie, A. H.; Raisin, C. G.; Thompson, J. W.; Wilson, C. L. *J. Chem. Soc.* **1936**, 971. (c) Redlich, O. Z. *Physik. Chem. B* **1935**, *28*, 371.

(29) Schafer, A.; Horn, H.; Ahlrichs, R. *J. Chem. Phys.* **1992**, *97*, 2571.

(30) (a) Klamt, A. *Quantum Chemistry to Fluid Phase Thermodynamics and Drug Design*; Elsevier: Amsterdam, 2005. (b) Klamt, A.; Jonas, V.; Burger, T.; Lohrenz, J. C. W. *J. Phys. Chem. A* **1998**, *102*, 5074. Klamt, A.; Schüürmann, G. *J. Chem. Soc., Perkin Trans.* **1993**, *2*, 799.

(31) Best, S. P.; Armstrong, R. S.; Beattie, J. K. *Inorg. Chem.* **1980**, *19*, 1958.

(32) Cotton, F. A.; Daniels, L. M.; Murillo, C. A.; Quesada, J. F. *Inorg. Chem.* **1993**, *32*, 4861.

(33) Blanchard, M.; Poitrasson, F.; Méheut, M.; Lazzeri, M.; Mauri, F.; Balan, E. *Geochim. Cosmochim. Acta* **2009**, *73*, 6565–6578.

(34) Dang, M. Z.; Rancourt, D. G.; Dutrizac, J. E.; Lamarche, G.; Provencher, R. *Hyperfine Interact.* **1998**, *117*, 271.

(35) Casey, W. H. *Chem. Rev.* **2006**, *106*, 1.

(36) (a) Casey, W. H.; Rustad, J. R. *Ann. Rev. Earth Planet. Sci.* **2007**, *35*, 21. (b) Wang, J. W.; Rustad, J. R.; Casey, W. H. *Inorg. Chem.* **2007**, *46*, 2962.

(37) Brown, G. E.; Henrich, V. E.; Casey, W. H.; Clark, D. L.; Eggleston, C.; Felmy, A. R.; Goodman, D. W.; Gratzel, M.; Maciel, G.; McCarthy, M. I.; Nealson, K. H.; Sverjensky, D. A.; Toney, M. F.; Zachara, J. M. *Chem. Rev.* **1999**, *99*, 77.

JP9065373